*J. Fluid Mech.* (2014), *vol.* 758, *pp.* 221–237.  
doi:10.1017/jfm.2014.527

# Dynamics of viscous liquid within a closed elastic cylinder subject to external forces with application to soft robotics

**S. B. Elbaz**[1] **and A. D. Gat**[1,†]

[1]Faculty of Mechanical Engineering, Technion – Israel Institute of Technology, Haifa 32000, Israel

(Received 13 January 2014; revised 11 April 2014; accepted 4 September 2014)

Viscous flows in contact with elastic structures apply both pressure and shear stress at the solid–liquid interface and thus create internal stress and deformation fields within the solid structure. We study the interaction between the deformation of elastic structures, subject to external forces, and an internal viscous liquid. We neglect inertia in the liquid and solid and focus on viscous flow through a thin-walled slender elastic cylindrical shell as a basic model of a soft robot. Our analysis yields an inhomogeneous linear diffusion equation governing the coupled viscous–elastic system. Solutions for the flow and deformation fields are obtained in closed analytical form. The functionality of the viscous–elastic diffusion process is explored within the context of soft-robotic applications, through analysis of selected solutions to the governing equation. Shell material compressibility is shown to have a unique effect in inducing different flow and deformation regimes. This research may prove valuable to applications such as micro-swimmers, micro-autonomous systems and soft robotics by allowing for the design and control of complex time-varying deformation fields.

**Key words:** low-Reynolds-number flows, lubrication theory

## 1. Introduction

Viscous flows within a solid body apply both pressure and shear stress at the solid–liquid interface and thus create stress and deformation fields within the solid structure, which in turn affect the flow field. The interaction between low-Reynolds-number liquid flow and the deformation of solid structures is relevant to various research areas such as instabilities in micro-fabrication processes (Al-Housseiny, Christov & Stone 2013), self-folding of solid sheets (commonly referred to as capillary origami, studied by Py *et al.* 2007; Pineirua, Bico & Roman 2010; Antkowiak *et al.* 2011), densification of patterned arrays of carbon nanotubes (studied by Huang *et al.* 2007; Zhao *et al.* 2010; De Volder *et al.* 2011), self-assembly and modification of the mechanical and geometrical properties of arrays of solid structures (studied by Chandra *et al.* 2009; Pokroy *et al.* 2009; Elwenspoek *et al.* 2010; Duprat, Aristoff & Stone 2011; Kang *et al.* 2011; Gat & Gharib 2013), biological flows (Toppaladoddi & Balmforth 2014) and soft robotics (Steltz *et al.* 2009; Ilievski *et al.* 2011; Shepherd *et al.* 2011; Martinez *et al.* 2012; Marchese, Onal & Rus 2014).

† Email address for correspondence: amirgat@technion.ac.il

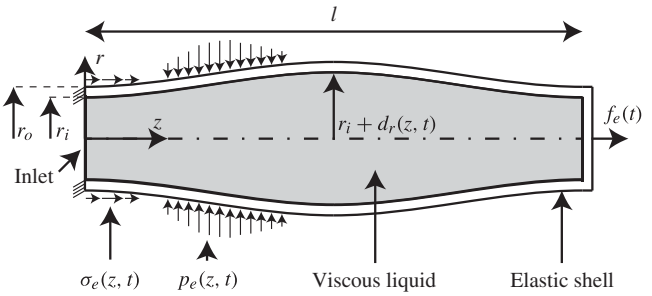


FIGURE 1. A schematic description of the elastic shell, the coordinate system and the external stress. The radial and axial coordinates are $r$ and $z$, respectively. The undeformed inner and outer cylinder radii are $r_i$ and $r_o$, respectively. The shell is clamped at $z = 0$ and free at $z = l$. The external stress components acting on the cylinder are radial stress $p_e$, shear stress $\sigma_e$ and an external axial force $f_e$ acting at $z = l$.

The interaction between fluid and solid dynamics for the case of viscous flow through elastic cylinders has been studied extensively in the context of collapsible tubes (e.g. Heil & Pedley 1995; Lowe & Pedley 1995; Heil 1996, 1997, 1998), studies of pipes conveying fluid (e.g. Païdoussis 1998) and flows in arteries (e.g. Canic & Mikelic 2003). The current study brings forth an analysis of the viscous–elastic interaction problem of a closed axisymmetric shell containing a viscous liquid. The aim of this work is to apply models and methods used in the study of biological flows to study time-varying deformation patterns in soft robotics (such as Shepherd *et al.* 2011; Morin *et al.* 2012; Martinez *et al.* 2013; Shepherd *et al.* 2013; Stokes *et al.* 2013).

## 2. Analysis

### 2.1. *Problem definition*

We study the fluid–structure interaction dynamics of viscous, Newtonian, incompressible flow through a slender linearly elastic cylinder (see figure 1) with negligible inertia of the liquid and solid. The relevant variables and parameters are time $t$, axial coordinate $z$, radial coordinate $r$, axial liquid speed $u_z$, radial liquid speed $u_r$, liquid pressure $p$, liquid viscosity $\mu$, solid radial deformation $d_r$, solid axial deformation $d_z$, solid strain $e_{ij}$ and stress $\sigma_{ij}$ (acting on the plane normal to coordinate $i$ and in the direction of coordinate $j$), solid Young's modulus $E$, solid Poisson's ratio $\nu$, inner cylinder radius $r_i$, outer cylinder radius $r_o$ and cylinder length $l$. An arbitrary external stress and pressure field is applied on the cylinder at $r = r_o + d_r$, defined by $\sigma_e = \sigma_{zr}(r = r_o + d_r, z, t)$ and $p_e = -\sigma_{rr}(r = r_o + d_r, z, t)$, respectively. An axial force $f_e(t)$ is applied at $z = l$.

We define the small parameter $\varepsilon_1$ representing the slenderness of the cylinder,

$$\varepsilon_1 = \frac{r_i}{l} \ll 1, \tag{2.1}$$

the small parameter $\varepsilon_2$ representing the thinness of the cylinder wall,

$$\varepsilon_2 = \frac{r_o - r_i}{r_i} \ll 1 \tag{2.2}$$

and the small parameter $\varepsilon_3$ representing small deformations of the solid,

$$\varepsilon_3 = \frac{d_r^*}{r_o} \sim \frac{d_z^*}{l} \ll 1, \tag{2.3}$$

where $d_r^*$ is the characteristic radial deformation and $d_z^*$ is the characteristic axial deformation. Normalized variables are hereafter denoted by uppercase letters and characteristic values are denoted by asterisks.

### 2.2. *Elastic problem*

The governing equations for axisymmetric linearly elastic material with negligible inertia and small deformations are (Mollmann 1981) conservation of momentum in the $r$ and $z$ directions,

$$\frac{\partial}{\partial r}(r\sigma_{rr}) + \frac{\partial}{\partial z}(r\sigma_{zr}) - \sigma_{\theta\theta} = 0, \tag{2.4}$$

$$\frac{\partial}{\partial r}(r\sigma_{zr}) + \frac{\partial}{\partial z}(r\sigma_{zz}) = 0, \tag{2.5}$$

respectively, the strain–displacement relations,

$$e_{rr} = \frac{\partial d_r}{\partial r}, \tag{2.6}$$

$$e_{\theta\theta} = \frac{d_r}{r}, \tag{2.7}$$

$$e_{zz} = \frac{\partial d_z}{\partial z}, \tag{2.8}$$

$$e_{zr} = \frac{1}{2}\left(\frac{\partial d_r}{\partial z} + \frac{\partial d_z}{\partial r}\right) \tag{2.9}$$

and Hooke's law,

$$Ee_{zz} = \sigma_{zz} - \nu(\sigma_{rr} + \sigma_{\theta\theta}), \tag{2.10}$$

$$Ee_{rr} = \sigma_{rr} - \nu(\sigma_{zz} + \sigma_{\theta\theta}), \tag{2.11}$$

$$Ee_{\theta\theta} = \sigma_{\theta\theta} - \nu(\sigma_{rr} + \sigma_{zz}), \tag{2.12}$$

$$Ee_{zr} = (1+\nu)\sigma_{zr}. \tag{2.13}$$

The boundary conditions representing the stress applied by the liquid and the external stress are

$$\sigma_{rr}(r = r_i) = p, \tag{2.14}$$

$$\sigma_{rr}(r = r_o + d_r) = -p_e, \tag{2.15}$$

$$\sigma_{zr}(r = r_i + d_r) = -\mu\frac{\partial u_z}{\partial r}, \tag{2.16}$$

$$\sigma_{zr}(r = r_o + d_r) = \sigma_e. \tag{2.17}$$

Here we have omitted the term $-2\mu\partial u_r/\partial r$ in (2.14) and the term $-\mu\partial u_r/\partial z$ in (2.16) since these terms are negligible compared with $p$ and $\partial u_z/\partial r$, respectively (this can be obtained by substitution of characteristic values from § 2.3 and is utilized in § 2.2 to simplify the derivation).

Following elastic shell theory (Gibson 1965; Mollmann 1981), we define stress resultants for the forces $n_{ij}$ as

$$n_{ij} = \int_{r_i}^{r_o} \sigma_{ij} \mathrm{d}r, \tag{2.18}$$

and moments $m_{ij}$ as

$$m_{ij} = \int_{r_i}^{r_o} \sigma_{ij} r \mathrm{d}r. \tag{2.19}$$

We define the normalized coordinates,

$$Z = \frac{z}{l}, \quad R = \frac{r}{r_i}, \tag{2.20a,b}$$

normalized stresses and pressure,

$$\Sigma_{rr} = \frac{\sigma_{rr}}{p^*}, \quad \Sigma_{zr} = \frac{\sigma_{zr}}{\varepsilon_1 p^*}, \quad P = \frac{p}{p^*} \tag{2.21a–c}$$

and normalized deformations,

$$D_r = \frac{d_r}{d_r^*}, \quad D_z = \frac{d_z}{d_z^*}, \tag{2.22a,b}$$

where $p^*$ is the characteristic pressure drop, $Z$ is the normalized axial coordinate, $R$ is the normalized radial coordinate, $\Sigma_{ij}$ is the normalized stress, $D_r$ and $D_z$ are the normalized radial and axial deflections and $P$ is the normalized liquid pressure. The externally applied forces are normalized accordingly,

$$P_e = \frac{p_e}{p^*}, \quad \Sigma_e = \frac{\sigma_e}{\varepsilon_1 p^*}, \quad F_e = \frac{f_e}{p^* \pi r_i^2}. \tag{2.23a–c}$$

We normalize the resultant $N_{zz} = n_{zz}/r_i p^*$. The normalized time is $T = t/t^*$, where the characteristic time $t^*$ is to be obtained by relation to the fluidic analysis. To obtain the equilibrium conditions in terms of resultants, we integrate the axial momentum equation with regard to $z$. Force balance in the axial direction yields

$$N_{zz}(Z, T) = \frac{P(Z, T) - KP(1, T) + F_e(T)}{2} + \int_Z^1 \Sigma_e(\zeta, T) \mathrm{d}\zeta, \tag{2.24}$$

where $K = 0$ for a closed boundary at $Z = 1$ (as illustrated in figure 1) and $K = 1$ for an open boundary at $Z = 1$. The term $KP(1, T)$ in (2.24) appears due to the axial force balance requirement at the clamped end, $Z = 0$.

In order to relate (2.5) into (2.4), we derive (2.5) with regards to $z$, multiply the axial momentum equilibrium equation by $r - r_m$ (where $r_m = (r_i + r_o)/2$) and integrate (2.5) with regard to $r$ from $r_i$ to $r_o$,

$$\frac{\partial n_{zr}}{\partial z} \sim \frac{\partial^2 m_{zz}}{\partial z^2} + r_o \frac{\partial \sigma_e}{\partial z} - r_i \frac{\partial \sigma_{zr}(r_i)}{\partial z}. \tag{2.25}$$

By integrating the radial momentum equation,

$$r_i p - r_o p_e + r_i \frac{\partial n_{zr}}{\partial z} - n_{\theta\theta} = 0, \tag{2.26}$$

we can substitute (2.25) into (2.26) to eliminate $\partial n_{zr}/\partial z$ and obtain

$$r_i p - r_o p_e + r_i \left( \frac{\partial^2 m_{zz}}{\partial z^2} + r_o \frac{\partial \sigma_e}{\partial z} - r_i \frac{\partial \sigma_{zr}(r_i)}{\partial z} \right) - n_{\theta\theta} \sim 0. \tag{2.27}$$

Normalizing (2.27) we thus obtain the leading-order relation,

$$P - P_e - N_{\theta\theta} \sim O(\varepsilon_1^2), \tag{2.28}$$

where $n^*_{\theta\theta} = r_i p^*$ and $N_{\theta\theta} = n_{\theta\theta}/r_i p^*$. We define $\sigma^*_{rr} = p^*$ (where $\sigma^*_{zz} = \sigma^*_{\theta\theta} = p^*/\varepsilon_2$) and thus Hooke's law can be used to establish the following strain–stress relations,

$$\Sigma_{zz} \sim \frac{\varepsilon_2 E}{p^*(1-\nu^2)} (e_{zz} + \nu e_{\theta\theta}) \tag{2.29}$$

and

$$\Sigma_{\theta\theta} \sim \frac{\varepsilon_2 E}{p^*(1-\nu^2)} (e_{\theta\theta} + \nu e_{zz}), \tag{2.30}$$

representing Love's first approximation (Love 1888). Following shell theory (Dugdale & Ruiz 1971), we apply the Kirchhoff hypothesis and describe the displacement field in terms of the radial $\bar{d}_r$ and axial $\bar{d}_z$ displacements of the mid-section, denoted by overbars,

$$\bar{d}_z = d_z - (r - r_m) \frac{\partial d_r}{\partial z}, \quad \bar{d}_r = d_r \tag{2.31a,b}$$

and thus we can represent the strain as a function of the deformation by

$$e_{zz} = \frac{\partial \bar{d}_z}{\partial z} - (r - r_m) \frac{\partial^2 \bar{d}_r}{\partial z^2}, \quad e_{\theta\theta} = \frac{\bar{d}_r}{r} \tag{2.32a,b}$$

and express the resultants in terms of deformation,

$$N_{zz} \sim \frac{E\varepsilon_2\varepsilon_3}{p^*(1-\nu^2)} \left( \frac{\partial \bar{D}_z}{\partial Z} + \nu \bar{D}_r \right), \tag{2.33}$$

$$N_{\theta\theta} \sim \frac{E\varepsilon_2\varepsilon_3}{p^*(1-\nu^2)} \left( \nu \frac{\partial \bar{D}_z}{\partial Z} + \bar{D}_r \right). \tag{2.34}$$

We now utilize (2.24) and (2.33) to define $\partial \bar{D}_z/\partial Z$ in terms of $\bar{D}_r$,

$$\frac{\partial \bar{D}_z}{\partial Z} = \frac{p^*(1-\nu^2)}{E\varepsilon_2\varepsilon_3} \left( \frac{P(Z,T) - KP(1,T) + F_e(T)}{2} + \int_Z^1 \Sigma_e(\zeta, T) \mathrm{d}\zeta \right) - \nu \bar{D}_r. \tag{2.35}$$

From order-of-magnitude we obtain

$$\frac{d^*_r}{r_i} = \frac{p^*}{E\varepsilon_2}, \tag{2.36}$$

which relates the requirement of small deformations to the characteristic pressure. We substitute (2.34) and (2.35) into (2.28) to obtain a governing equation for the radial

deflection $\bar{D}_r$,

$$\bar{D}_r(Z,T) \sim P(Z,T) - P_e - \nu\left(\frac{P(Z,T) - KP(1,T) + F_e(T)}{2} + \int_Z^1 \Sigma_e(\zeta,T)\mathrm{d}\zeta\right), \tag{2.37}$$

which substituted into (2.35) yields the corresponding relation for the axial deflection $\bar{D}_z$,

$$\frac{\partial \bar{D}_z}{\partial Z} = \frac{P(Z,T) - KP(1,T) + F_e(T)}{2} + \int_Z^1 \Sigma_e(\zeta,T)\mathrm{d}\zeta - \nu(P(Z,T) - P_e(Z,T)). \tag{2.38}$$

### 2.3. *Fluidic problem*

The governing equations for axisymmetric incompressible Newtonian flow are momentum conservation in the $r$ and $z$ directions,

$$\rho\left(\frac{\partial u_r}{\partial t} + u_r\frac{\partial u_r}{\partial r} + u_z\frac{\partial u_r}{\partial z}\right) = -\frac{\partial p}{\partial r} + \mu\left[\frac{1}{r}\frac{\partial}{\partial r}\left(r\frac{\partial u_r}{\partial r}\right) + \frac{\partial^2 u_r}{\partial z^2} - \frac{u_r}{r^2}\right], \tag{2.39}$$

$$\rho\left(\frac{\partial u_z}{\partial t} + u_r\frac{\partial u_z}{\partial r} + u_z\frac{\partial u_z}{\partial z}\right) = -\frac{\partial p}{\partial z} + \mu\left[\frac{1}{r}\frac{\partial}{\partial r}\left(r\frac{\partial u_z}{\partial r}\right) + \frac{\partial^2 u_z}{\partial z^2}\right] + \rho g, \tag{2.40}$$

respectively, and conservation of mass,

$$\frac{1}{r}\frac{\partial}{\partial r}(ru_r) + \frac{\partial u_z}{\partial z} = 0. \tag{2.41}$$

The boundary conditions are no-slip and no-penetration at the solid–liquid interface,

$$u_r(r = r_i + d_r) = \frac{\partial d_r}{\partial t}, \quad u_z(r = r_i + d_r) = \frac{\partial d_z}{\partial t} \tag{2.42a,b}$$

and pressure at the inlet

$$p(z = 0) = p_0(t), \tag{2.43}$$

where $p_0(t)$ is an arbitrary function of time. We define the normalized axial and radial speeds,

$$U_z = \frac{u_z}{u_z^*}, \quad U_r = \frac{u_r}{u_r^*}, \tag{2.44a,b}$$

and order-of-magnitude analysis of (2.41) yields

$$\frac{u_r^*}{u_z^*} \sim \frac{r_i}{l} = \varepsilon_1, \quad u_z^* = \frac{\varepsilon_1 r_i p^*}{\mu}. \tag{2.45}$$

We define normalized gravity as $G = \rho g l/p^*$. Substituting (2.45) into (2.39)–(2.41) and normalizing yields

$$\frac{\partial P}{\partial Z} = \frac{1}{R}\frac{\partial}{\partial R}\left(R\frac{\partial U_z}{\partial R}\right) + G + O\left(\varepsilon_1^2, \frac{\rho r_i^2}{\mu t^*}\right), \tag{2.46}$$

$$\frac{\partial P}{\partial R} = O\left(\varepsilon_1^2, \frac{\varepsilon_1^2 \rho r_i^2}{\mu t^*}\right) \tag{2.47}$$

and

$$\frac{\partial U_z}{\partial Z} + \frac{1}{R}\frac{\partial}{\partial R}(RU_r) = 0. \tag{2.48}$$

Integrating (2.46) with regard to $R$ and applying (2.42) in normalized form, we attain

$$U_z \sim \frac{d_z^*}{t^* u_z^*}\frac{\partial D_z}{\partial T} + \frac{1}{4}\left(\frac{\partial P}{\partial Z} - G\right)[R^2 - (1 + \varepsilon_3 D_r(Z))^2]. \tag{2.49}$$

We thus obtain the characteristic time scale of the viscous–elastic interaction as

$$t^* = \frac{d_z^*}{u_z^*} = \frac{\mu}{E\varepsilon_2\varepsilon_1^2}, \tag{2.50}$$

balancing the pressure gradient term with the shell's axial motion term. Substituting (2.49) into (2.48) and integrating with regard to $R$ we obtain a relation between the liquid pressure field and the axial and radial deformations of the elastic shell,

$$\frac{1}{2}\frac{\partial^2 D_z}{\partial T \partial Z} - \frac{1}{16}\frac{\partial^2 P}{\partial Z^2} + \frac{\partial D_r}{\partial T} \sim 0. \tag{2.51}$$

### 2.4. *Fluidic–elastic problem*

We substitute (2.37) and (2.38) into (2.51) to obtain the governing equation for the fluidic pressure,

$$\frac{\partial P}{\partial T} - \frac{1}{4(5-4\nu)}\frac{\partial^2 P}{\partial Z^2} \sim \frac{2\nu - 1}{5 - 4\nu}\left(2\int_Z^1 \frac{\partial \Sigma_e}{\partial T}\mathrm{d}\zeta + \frac{\partial F_e}{\partial T} - K\frac{\partial P_1}{\partial T}\right) + \frac{4 - 4\nu}{5 - 4\nu}\frac{\partial P_e}{\partial T}, \tag{2.52}$$

with the initial condition $P(Z, 0) = P_i(Z)$ and appropriate boundary conditions. For the case of an inlet the boundary condition will take the form $P = P_0(T)$, whereas for the case of a closed boundary the condition will be $\partial P/\partial Z = G$.

The corresponding dimensional equation reads

$$\frac{\partial p}{\partial t} - \frac{\partial^2 p}{\partial z^2}\frac{Er_i(r_o - r_i)}{4(5-4\nu)\mu} = \frac{2\nu - 1}{5 - 4\nu}\left[\left(\frac{\partial f_e}{\partial t} + 2\pi r_i\int_z^l \frac{\partial \sigma_e}{\partial t}\mathrm{d}\zeta\right)\frac{1}{\pi r_i^2} - K\frac{\partial p(l, t)}{\partial t}\right] + \frac{\partial p_e}{\partial t}\frac{4 - 4\nu}{5 - 4\nu}. \tag{2.53}$$

From (2.50) and (2.36), the requirements of negligible inertia and small deformations can be expressed by the physical conditions,

$$\alpha^2 = \frac{\rho r_i^2}{\mu t^*} = \frac{E\varepsilon_2\varepsilon_1^2\rho r_i^2}{\mu^2} \ll 1, \quad \frac{d_r^*}{r_i} = \frac{p^*}{\varepsilon_2 E} \ll 1, \tag{2.54a,b}$$

respectively. The requirement for negligible inertia derived from the squared Womersley number, denoted by $\alpha^2$, depends only on the solid and liquid physical properties, and not on the external forces and stress applied on the configuration.

We note that for $\nu = 1/2$, corresponding to an incompressible solid, axial stress does not affect the pressure field within the liquid. In addition, for the case of an open boundary at $Z = 1$ the function $P_1(T)$ which describes the boundary condition also appears in the inhomogeneous part of the governing equation. This effect comes into play for $\nu < 1/2$ representing an added level of influence of solid compressibility on the fluidic pressure field. We also note that the Poisson's ratio dependent coefficients of (2.52) are smooth functions throughout the physical range $-1 < \nu < 1/2$.

## 3. Results

The governing equation (2.52) may be solved for a variety of boundary and initial conditions, representing external stresses acting on the cylinder or internal pressures at the inlet. After the calculation of the pressure $P$ by (2.52), the deformations $D_r$, $D_z$ can be calculated by (2.37) and (2.38) and the fluid mass-flux $Q$ can be calculated by integration of (2.49). In all cases the shell is clamped at $Z=0$ and gravity is neglected. We will present solutions for several scenarios relevant to soft robotics.

### 3.1. *Transient dynamics due to sudden forces*

Figures 2, 3 and 5 present the pressure, mass flux, radial deformation and axial deformation due to sudden forces acting on the cylinder. The boundary at $Z=0$ is open and the boundary at $Z=1$ is closed, $\partial P/\partial Z=0$. Figure 4 presents the settling time of the solution in the case of a spatially localized force as a function of its axial location. In all cases the initial conditions are $P(Z,0)=D_r(Z,0)=D_z(Z,0)=0$. Dashed lines denote incompressible solids, $\nu=0.5$ and solid lines denote compressible solids, $\nu=0.33$. Blue, red, green and magenta lines correspond to normalized time, $T=0.01,\ 0.1,\ 1$ and 10, respectively.

#### 3.1.1. *Sudden change of inlet pressure*

Change of the inlet pressure is the main mechanism used to actuate fluidic-based soft robots. Our analysis will include the transient viscous dynamics associated with the sudden increase of inlet pressure, so far neglected in the design of soft robots. The relevant boundary condition for this case is $P(0,T)=H(T)$, where $H(T)$ is the Heaviside function. Solution of (2.52) for this case yields

$$P(Z,T)=1-\frac{4}{\pi}\sum_{n=1}^{\infty}\frac{\sin\left[(2n-1)\pi Z/2\right]}{2n-1}\exp\left[-\frac{(2n-1)^2\pi^2}{16(5-4\nu)}T\right]. \tag{3.1}$$

Solution (3.1) is presented in figure 2. For $\nu=0.5$ the axial displacement (figure 2*d*) is 0 for all $T$, since the increase in deflection due to the axial stress by the liquid is of equal magnitude and opposite sign to the axial deflection emanating from the radial deflection $D_r$ (see (2.38)). This effect in $D_z$ corresponds to different behavior of the mass flux $Q$ within the cylinder for $\nu=0.5$ compared with $\nu=0.33$.

#### 3.1.2. *Sudden spatially localized radial force acting on the external shell*

An external force suddenly applied on a soft structure will create flow within the structure due to displacement of liquid driven by the solid deformation. The reaction to such a sudden force will be a viscous–elastic diffusion process. We examine a sudden axisymmetric radial force acting at $Z=3/4$ from time $T=T_s$. The relevant inhomogeneous term in (2.52) is $P_e(Z,T)=H(T-T_s)\Delta(Z-3/4)$, where $H(T)$ is the Heaviside function and $\Delta(Z)$ is Dirac's delta. The obtained solution of (2.52) for this case is

$$\begin{aligned}P(Z,T) \;=\; & H(T-T_s)\frac{8-8\nu}{5-4\nu}\sum_{n=1}^{\infty}\sin\left[\frac{(2n-1)\pi Z_s}{2}\right]\sin\left[\frac{(2n-1)\pi Z}{2}\right]\\ & \times\exp\left[-\frac{(2n-1)^2\pi^2}{16(5-4\nu)}(T-T_s)\right],\end{aligned} \tag{3.2}$$

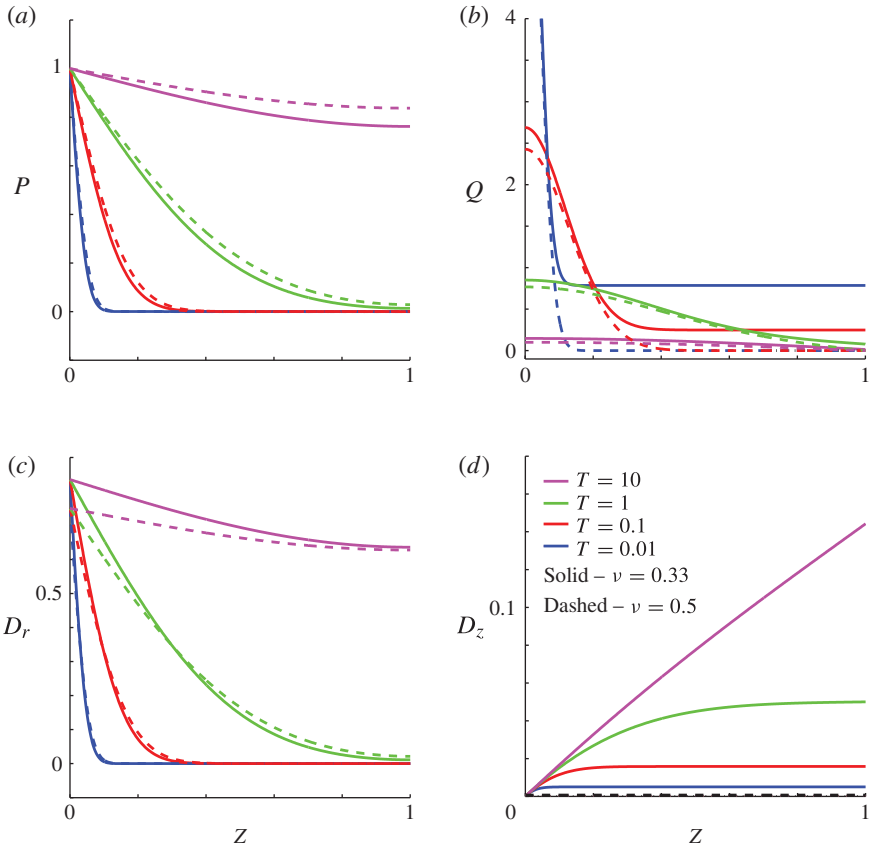


FIGURE 2. (Colour online) Viscous–elastic dynamics due to inlet pressure $P(0, T) = H(T)$, where $H(T)$ is the Heaviside function: (*a*) pressure versus axial coordinate; (*b*) mass flux versus axial coordinate; (*c*) radial deformation versus axial coordinate; (*d*) axial deformation versus axial coordinate. The initial conditions are $P(Z, 0) = D_r(Z, 0) = D_z(Z, 0) = 0$. The shell is open at $Z = 0$ and closed at $Z = 1$. The shell is clamped at $Z = 0$. Dashed lines denote incompressible solids, $\nu = 0.5$ and solid lines denote compressible solids, $\nu = 0.33$. Blue, red, green and magenta lines correspond to normalized time, $T = 0.01$, 0.1, 1 and 10, respectively. In (*d*) all dashed lines are at 0 for all $Z$ and are replaced by a single black dashed line.

where $(Z_s, T_s)$ are the location and time of the shock. Results are presented in figure 3. Initially a symmetric pressure is created around the location of the force, as $T$ increases the flux becomes negative as fluid exits the channel due to the change of volume. We note that for an incompressible solid ($\nu = 0.5$), in similar fashion to § 3.1.1, all $D_z$ lines fall on a single curve with a sudden jump at the location of the force. The radial deflection follows the same pattern as the pressure despite the singularity at $Z = 3/4$ resulting from the impact. We may examine the settling time of the solution, beyond which the initial state of equilibrium is regained. We define the state of equilibrium in terms of the radial displacement,

$$D_r(Z, T; Z_s) < \mathscr{A}_r^{eq}, \tag{3.3}$$

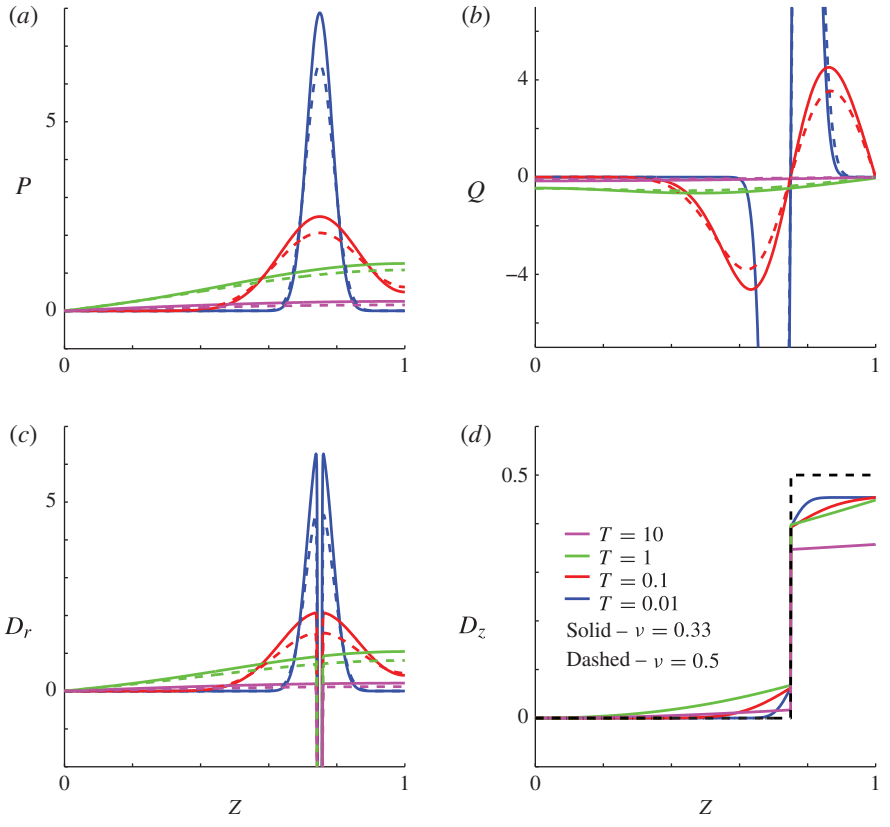


FIGURE 3. (Colour online) Viscous–elastic dynamics due to external radial pressure $P_e = H(T)\Delta(Z - 3/4)$, where $H(T)$ is the Heaviside function and $\Delta(Z)$ is Dirac's delta: (*a*) pressure versus axial coordinate; (*b*) mass flux versus axial coordinate; (*c*) radial deformation versus axial coordinate; (*d*) axial deformation versus axial coordinate. The shell is open at $Z = 0$ and closed at $Z = 1$. The shell is clamped at $Z = 0$. The initial conditions are $P(Z, 0) = D_r(Z, 0) = D_z(Z, 0) = 0$. Dashed lines denote incompressible solids, $\nu = 0.5$ and solid lines denote compressible solids, $\nu = 0.33$. Blue, red, green and magenta lines correspond to normalized time, $T = 0.01$, 0.1, 1 and 10, respectively. In (*d*) all dashed lines fall on a single curve and are replaced by a single black dashed line.

where for a given shock location $Z_s$ the radial displacement has fallen below a threshold amplitude of $\mathscr{A}_r^{eq}$, this definition is valid outside the singularity of $Z = Z_s$. A good approximation for the settling time $T_{eq}$ can be attained based on the first mode of the Fourier series (3.2) yielding

$$T_{eq}(Z_s) = \frac{16(5 - 4\nu)}{\pi^2} \log\left[\frac{8(1 - \nu)^2}{(5 - 4\nu)} \frac{\sin(\pi Z_s/2)}{\mathscr{A}_r^{eq}}\right]. \tag{3.4}$$

Figure 4 shows a comparison of the first mode and full series solution for both $\nu = 0.33$ and $\nu = 0.5$. A typical value of $\mathscr{A}_r^{eq} = 0.1$ was used, in which case the first mode approximation and numerical extraction are in unison as of $Z_s > 0.1$. As the location of the shock approaches the inlet the solution decays faster, thus for a given threshold $\mathscr{A}_r^{eq}$ additional modes of the sum must be taken into account.

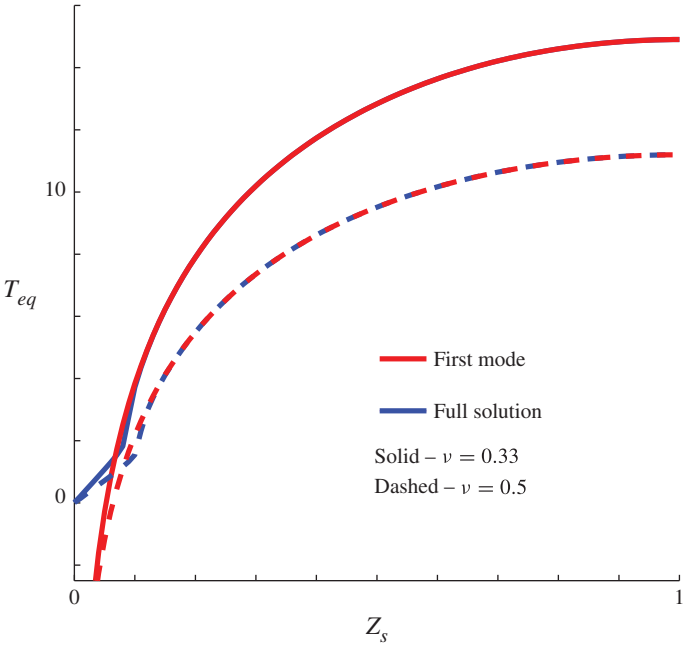


FIGURE 4. (Colour online) The settling time $T_{eq}$ to equilibrium state as a function of impact location $Z_s$ in the case of an external radial pressure $P_e = H(T - T_s)\Delta(Z - Z_s)$, where $H(T)$ is the Heaviside function and $\Delta(Z)$ is Dirac's delta. Dashed lines denote incompressible solids, $\nu = 0.5$, and solid lines denote compressible solids, $\nu = 0.33$. The numerical extraction (blue) is plotted alongside the first mode approximation (red) of (3.2) in the case of $\mathscr{A}_r^{eq} = 0.1$. Analytic approximation valid as of $Z_s > 0.1$.

3.1.3. *Sudden axial force acting at* $Z = 1$

In this case we examine a sudden axial force acting on the cylinder at $Z = 1$, corresponding to an impact with an external object, represented by $F_e = -H(T)$. The relevant solution of (2.52) for this case is

$$P(Z, T) = \frac{4(1-2\nu)}{\pi(5-4\nu)} \sum_{n=1}^{\infty} \frac{\sin\left[(2n-1)\pi Z/2\right]}{2n-1} \exp\left[-\frac{(2n-1)^2\pi^2}{16(5-4\nu)}T\right]. \tag{3.5}$$

Results are shown in figure 5. For $\nu = 0.33$ there is a sudden increase in pressure within the cylinder at $T = 0$ followed by deflation for $T > 0$. Here $P$ and $Q$ propagate similarly to the inflation case (figure 2), varying in magnitude and direction. For $\nu = 0.5$ the volume change due to axial deformation is canceled out by the volume change due to radial deformation and there is, remarkably, no effect on the pressure $P$ or flux $Q$ of the liquid within the cylinder. The radial deformation in the case of $\nu = 0.5$ is constant, a result of solid displacement alone. The axial deformation is nearly linear for both $\nu = 0.5$ and 0.33.

### 3.2. *Steady-state solution for oscillating inlet pressure*

Various practical applications may involve oscillations and periodic motions. We illustrate such a case with a closed boundary at $Z = 0$ and an open boundary

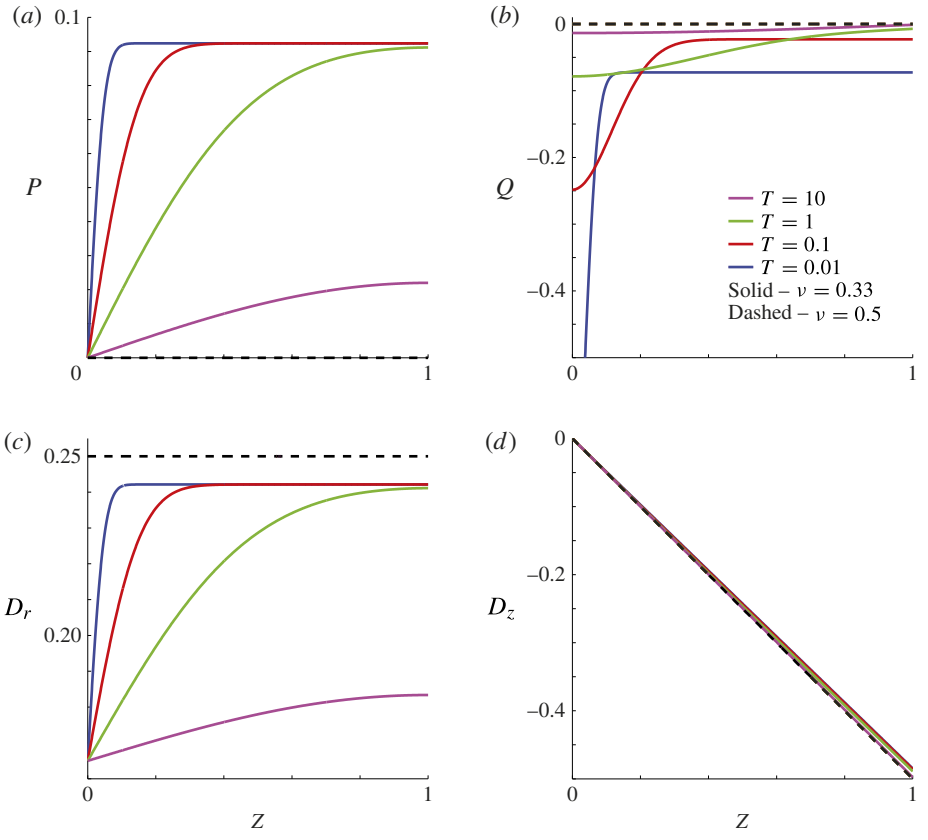


FIGURE 5. (Colour online) Viscous–elastic dynamics due to external axial force $F_e = -H(T)$, where $H(T)$ is the Heaviside function: (*a*) pressure versus axial coordinate; (*b*) mass flux versus axial coordinate; (*c*) radial deformation versus axial coordinate; (*d*) axial deformation versus axial coordinate. The initial conditions are $P(Z, 0) = D_r(Z, 0) = D_z(Z, 0) = 0$. The shell is open at $Z = 0$ and closed at $Z = 1$. The shell is clamped at $Z = 0$. Dashed lines denote incompressible solids, $\nu = 0.5$ and solid lines denote compressible solids, $\nu = 0.33$. Blue, red, green and magenta lines correspond to normalized time, $T = 0.01$, 0.1, 1 and 10, respectively. All dashed lines in this figure fall on a single curve and are replaced by a single black dashed line.

at $Z = 1$ ($K = 1$ in (2.52)). Corresponding boundary conditions are given by $\partial P(0, T)/\partial Z = 0$ and $P(1, T) = \cos(\Omega T)$, $\Omega$ representing the deviation from the base frequency of $1/t^*$. The shell is clamped at $Z = 0$. The initial conditions are $P(Z, 0) = D_r(Z, 0) = D_z(Z, 0) = 0$. The steady-state solution of (2.52) for these boundary conditions is given by

$$P(Z, T) = \mathrm{Re}\left\{\left[\frac{(4-2\nu)\cosh[Z(1+\mathrm{i})\sqrt{(10-8\nu)\Omega}]}{(5-4\nu)\cosh[(1+\mathrm{i})\sqrt{(10-8\nu)\Omega}]} + \frac{1-2\nu}{5-4\nu}\right]\exp(\mathrm{i}\Omega T)\right\}. \quad (3.6)$$

Figure 6 presents viscous–elastic dynamics due to oscillating pressure at $Z = 1$. In figure 6(*a–d*) $\Omega = 1$, in figure 6(*e–h*) $\Omega = 3$ and in figure 6(*i–l*) $\Omega = 30$. Solid lines (blue online) denote compressible solids ($\nu = 0.33$) and dashed lines (red online) denote incompressible solids ($\nu = 0.5$). Figure 6(*a*,*e*,*i*) present pressure versus

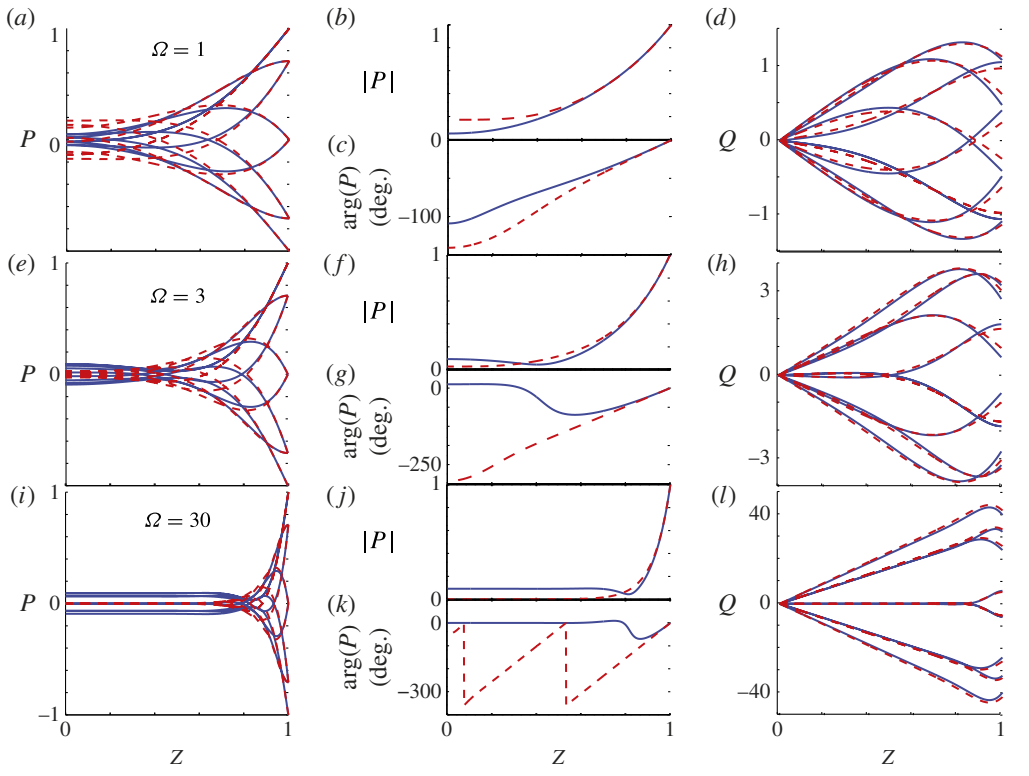


FIGURE 6. (Colour online) Viscous–elastic dynamics due to an oscillatory inlet boundary pressure at $Z=1$, $P(1,T)=\cos(\Omega T)$ and closed boundary at $Z=0$, $\partial P(0,T)/\partial Z=0$. The shell is clamped at $Z=0$. In (*a–d*) $\Omega=1$, in (*e–h*) $\Omega=3$ and in (*i–l*) $\Omega=30$. Solid lines (blue online) denote compressible solids, $\nu=0.33$ and dashed lines (red online) denote incompressible solids, $\nu=0.5$. In (*a*,*e*,*i*) the pressure is presented versus axial coordinate. In (*b*,*f*,*j*) wave amplitude is presented versus axial coordinate. In (*c*,*g*,*k*) wave phase is presented versus axial coordinate. In (*d*,*h*,*l*) the mass flux is presented versus the axial coordinate. For (*a*,*d*,*e*,*h*,*i*,*l*), eight lines are plotted evenly over a single time period.

axial coordinate. Figure 6(*b*,*f*,*j*) depict the wave amplitude versus axial coordinate. Figure 6(*c*,*g*,*k*) depict the wave phase versus axial coordinate. Figure 6(*d*,*h*,*l*) present mass flux versus axial coordinate. For figure 6(*a*,*d*,*e*,*h*,*i*,*l*), eight lines are plotted evenly over a single time period.

For $\Omega \ll 1$, for all values of $\nu$ the solution exhibits a spatially uniform pressure regime, the common mode in current soft-robotic applications. For $\Omega = 1$ (figure 6*a–d*), the base frequency of the system, we observe a growing phase diffusion for both $\nu=0.33$ and 0.5, where for $\nu=0.5$ pressure oscillations are less damped. For $\Omega=3$ (figure 6*e–h*) we observe antiphase pressure oscillations past a contraction region of the oscillations for $\nu=0.33$, but not for $\nu=0.5$, where for $\nu=0.33$ pressure oscillations are less damped. For $\Omega=30\gg1$ (figure 6*i–l*) the pressure contraction is amplified and for $\nu=0.5$ the pressure oscillations are limited to a length scale of the order of $\approx r_i\sqrt{E\varepsilon_2 t^*/\mu}$ (the natural length scale of the externally forced time scale $t^*/\Omega$, see (2.50)). For $\nu=0.33$ the pressure oscillations past the contraction are not damped, regardless of inlet pressure frequency. Thus, high-frequency oscillations can be applied and detected for $\nu=0.33$ but not $\nu=0.5$.

### 3.3. *Solutions for a fully closed shell*

The case of a cylindrical shell closed at both boundaries ($Z = 0$ and $Z = 1$) and clamped at $Z = 0$ is represented by the Neumann boundary condition on the pressure field, $\partial P(0, T)/\partial Z = \partial P(1, T)/\partial Z = 0$ ($K = 0$ in (2.52)). We are interested in the viscous–elastic dynamics as a result of external impact or actuation. We first examine axial imposition of the shell at $Z = 1$ prescribed by an arbitrary forcing term $F_e = -f(T)$ in (2.52). The solution for the internal pressure field in this case is simply,

$$P(Z, T) = \frac{1 - 2\nu}{5 - 4\nu} f(T), \tag{3.7}$$

a reproduction of the external forcing. Solving for the radial and axial displacements yields

$$D_r(Z, T) = \frac{\nu^2 - 1}{4\nu - 5} f(T), \quad D_z(Z, T) = -2\frac{\nu^2 - 1}{4\nu - 5} Z f(T). \tag{3.8a,b}$$

We note that the volume of the shell is conserved during its motion, as expected of the incompressible liquid confined within it. By reason of negligible inertia in the solid the imposition of the wall at $Z = 1$ produces a uniform motion of the solid experienced accordingly by the liquid. We illustrate a spatially localized impact with analogous conditions to those of § 3.1.2. The solution of (2.52) under the Neumann boundary condition is given by

$$P(Z, T) = H(T - T_s)\frac{4 - 4\nu}{5 - 4\nu}\left[1 + 2\sum_{n=1}^{\infty} \cos(n\pi Z_s)\cos(n\pi Z)\exp\left(-\frac{n^2\pi^2(T - T_s)}{4(5 - 4\nu)}\right)\right], \tag{3.9}$$

where $(Z_s, T_s)$ are the location and time of the shock. Results are shown in figure 7. The localized displacement near the impact, previously diffused by the shell (see § 3.1.2) is now translated to a steady-state solution in pressure, radial and axial deflections (compared with figure 3). This effect also causes significant steady-state stretching of the shell left of the impact, which does not occur in the case of an open boundary at $Z = 0$.

## 4. Concluding remarks

We studied the time-dependent interaction between viscous flow within an elastic cylindrical shell and the deformation of the shell in the context of soft-robotic applications. Utilizing order-of-magnitude analysis and elastic shell theory we obtained a leading-order diffusion equation relating external forces acting on the cylinder, the inlet pressure and the pressure distribution within the channel.

From the normalization of the governing equations we obtained the condition $\alpha^2 = E\varepsilon_2\varepsilon_1^2\rho r_i^2/\mu^2 \ll 1$ for inertial effects to be negligible. This condition represents the ratio between the relevant inertial–viscous time scale $\rho r_i^2/\mu$ and the viscous–elastic time scale $t^* = \mu/E\varepsilon_2\varepsilon_1^2$. The characteristic speed of the viscous–elastic interaction is given by $l/t^* = \sqrt{\alpha^2\varepsilon_2 E/\rho}$. Examining configurations with constant geometric proportions, $\varepsilon_1 = 0.01$ and $\varepsilon_2 = 0.1$, and demanding that $\alpha^2 < 0.1$, we may derive the maximal value of $r_i$ for which the assumption of negligible inertia is valid. The corresponding maximal propagation speed $l/t^*$ may be attained in the same manner. Highly viscous liquids such as silicone oil ($\rho = 0.75 \times 10^3$ kg m$^{-3}$, $\mu = 60$ Pa s) when interacting with soft materials such as PDMS (polydimethylsiloxane; $E = 4 \times 10^5$ Pa) yield limiting upper values of $r_i \approx 0.3$ m and $l/t^* \approx 1$ m s$^{-1}$. Silicon oil interacting

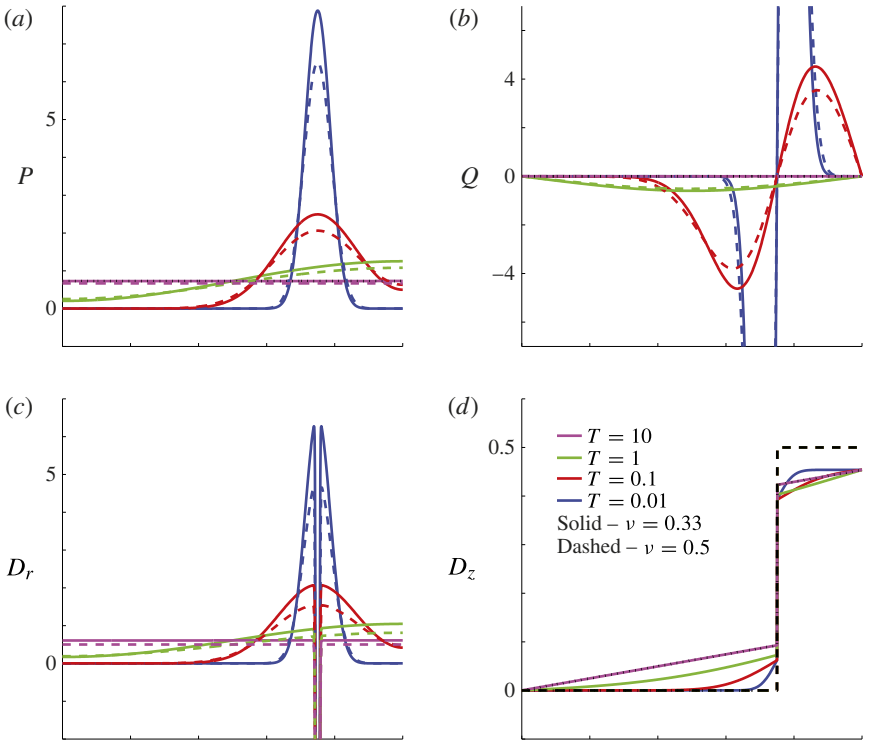


FIGURE 7. (Colour online) Viscous–elastic dynamics of a fully closed shell due to external radial pressure $P_e = H(T - T_s)\Delta(Z - 3/4)$, where $H(T)$ is the Heaviside function and $\Delta(Z)$ is Dirac's delta: (*a*) pressure versus axial coordinate; (*b*) mass flux versus axial coordinate; (*c*) radial deformation versus axial coordinate; (*d*) axial deformation versus axial coordinate. The initial conditions are $P(Z, 0) = D_r(Z, 0) = D_z(Z, 0) = 0$. The shell is clamped at $Z = 0$. Dashed lines denote incompressible solids, $\nu = 0.5$ and solid lines denote compressible solids, $\nu = 0.33$. Blue, red, green and magenta lines correspond to normalized time, $T = 0.01$, 0.1, 1 and 10, respectively. In (*d*) all dashed lines fall on a single curve and are replaced by a single black dashed line.

with more rigid materials, such as aluminum ($E = 6.9 \times 10^{10}$ Pa), yields values of $r_i \approx 10^{-3}$ m and $l/t^* \approx 500$ m s$^{-1}$. For water ($\rho = 10^3$ kg m$^{-3}$, $\mu = 10^{-3}$ Pa s) we obtain a maximal inner radius of $r_i \approx 5 \times 10^{-6}$ m even when interacting with soft materials such as PDMS, limiting the validity of the analysis in the case of water and less-viscous liquids to flows in soft micro-geometries. For a more slender and thinner shell geometry the upper limit on $r_i$ will be relaxed in inverse proportion to $\sqrt{\varepsilon_2}\varepsilon_1$, increasing the range of validity of the model.

Our analysis revealed that in the case of an incompressible material ($\nu = 0.5$), the effects of external axial force $F_e$ and external shear stress $\Sigma_e$ are eliminated from the governing equation. Solution to the pressure, velocity and deformation fields of the coupled viscous–elastic system induced by sudden application of external (radial or axial) stress has been attained in closed form, as well as solutions for sudden change in inlet pressure and oscillating inlet pressure. Corresponding solutions for the case of an externally forced fully closed shell have also been attained. In the case of a compressible shell ($\nu = 0.33$) an antiphase pressure regime has been observed in response to inlet pressure oscillating at frequencies higher than $1/t^*$. The oscillations

occur passed a contraction region beyond which the corresponding incompressible shell ($\nu = 0.5$) solution has decayed. This research may be used as a basis for the design and control of a time-varying deformation field in soft-robotic applications.

**Acknowledgement**

This research was supported by the Israel Science Foundation (grant no. 818/13).

## REFERENCES

AL-HOUSSEINY, T. T., CHRISTOV, I. C. & STONE, H. A. 2013 Two-phase fluid displacement and interfacial instabilities under elastic membranes. *Phys. Rev. Lett.* **111** (3), 034502.

ANTKOWIAK, A., AUDOLY, B., JOSSERAND, C., NEUKIRCH, S. & RIVETTI, M. 2011 Instant fabrication and selection of folded structures using drop impact. *Proc. Natl Acad. Sci. USA* **108**, 10400–10404.

CANIC, S. & MIKELIC, A. 2003 Effective equations modeling the flow of a viscous incompressible fluid through a long elastic tube arising in the study of blood flow through small arteries. *SIAM J. Appl. Dyn. Syst.* **2** (3), 431–463.

CHANDRA, D., YANG, S., SOSHINSKY, A. A. & GAMBOGI, R. J. 2009 Biomimetic ultrathin whitening by capillary-force-induced random clustering of hydrogel micropillar arrays. *ACS Appl. Mater. Interfaces* **1**, 1698–1704.

DE VOLDER, M. F. L., PARK, S. J., TAWFICK, S. H., VIDAUD, D. O. & HART, A. J. 2011 Fabrication and electrical integration of robust carbon nanotube micropillars by self-directed elastocapillary densification. *J. Micromech. Microengng* **21**, 045033.

DUGDALE, D. S. & RUIZ, C. 1971 *Elasticity for Engineers*. McGraw-Hill.

DUPRAT, C., ARISTOFF, J. M. & STONE, H. A. 2011 Dynamics of elastocapillary rise. *J. Fluid Mech.* **679**, 641–654.

ELWENSPOEK, M., ABELMANN, L., BERENSCHOT, E., VAN HONSCHOTEN, J., JANSEN, H. & TAS, N. 2010 Self-assembly of (sub-)micron particles into supermaterials. *J. Micromech. Microengng* **20**, 064001.

GAT, A. D. & GHARIB, M. 2013 Elasto-capillary coalescence of multiple parallel sheets. *J. Fluid Mech.* **723**, 692–705.

GIBSON, J. E. 1965 *Linear Elastic Theory of Thin Shells*. Pergamon Press.

HEIL, M. 1996 The stability of cylindrical shells conveying viscous flow. *J. Fluids Struct.* **10**, 173–196.

HEIL, M. 1997 Stokes flow in collapsible tubes – computation and experiment. *J. Fluid Mech.* **353**, 285–312.

HEIL, M. 1998 Stokes flow in an elastic tube – a large-displacement fluid–structure interaction problem. *Intl J. Numer. Meth. Fluids* **28**, 243–265.

HEIL, M. & PEDLEY, T. J. 1995 Large axisymmetric deformations of a cylindrical shell conveying a viscous flow. *J. Fluids Struct.* **9**, 237–256.

HUANG, X., ZHOU, J., SANSOM, E., GHARIB, M. & HAUR, S. C. 2007 Inherent opening controlled pattern formation in carbon nanotube arrays. *Nanotechnology* **18**, 305301.

ILIEVSKI, F., MAZZEO, A. D., SHEPHERD, R. F., CHEN, X. & WHITESIDES, G. M. 2011 Soft robotics for chemists. *Angew. Chem.* **123** (8), 1930–1935.

KANG, S. H., WU, N., GRINTHAL, A. & AIZENBERG, J. 2011 Meniscus lithography: evaporation-induced self-organization of pillar arrays into Moiré patterns. *Phys. Rev. Lett.* **107**, 177802.

LOVE, A. E. H. 1888 The small free vibrations and deformations of a thin elastic shell. *Phil. Trans. R. Soc. Lond.* A **179**, 491–546.

LOWE, T. W. & PEDLEY, T. J. 1995 Computation of Stokes flow in a channel with a collapsible segment. *J. Fluids Struct.* **9** (8), 885–905.

MARCHESE, A. D., ONAL, C. D. & RUS, D. 2014 Autonomous soft robotic fish capable of escape maneuvers using fluidic elastomer actuators. *Soft Robot.* **1** (1), 75–87.

MARTINEZ, R. V., BRANCH, J. L., FISH, C. R., JIN, L., SHEPHERD, R. F., NUNES, R., SUO, Z. & WHITESIDES, G. M. 2013 Robotic tentacles with three-dimensional mobility based on flexible elastomers. *Adv. Mater.* **25** (2), 205–212.

MARTINEZ, R. V., FISH, C. R., CHEN, X. & WHITESIDES, G. M. 2012 Elastomeric origami: programmable paper-elastomer composites as pneumatic actuators. *Adv. Funct. Mater.* **22** (7), 1376–1384.

MOLLMANN, H. 1981 *Introduction to the Theory of Thin Shells*. John Wiley & Sons.

MORIN, S. A., SHEPHERD, R. F., KWOK, S. W., STOKES, A. A., NEMIROSKI, A. & WHITESIDES, G. M. 2012 Camouflage and display for soft machines. *Science* **337** (6096), 828–832.

PAÏDOUSSIS, M. P. 1998 *Fluid–Structure Interactions, Slender Structures and Axial Flow*. Academic Press.

PINEIRUA, M., BICO, J. & ROMAN, B. 2010 Capillary origami controlled by an electric field. *Soft Matt.* **6**, 4491–4496.

POKROY, B., KANG, S. H., MAHADEVAN, L. & AIZENBERG, J. 2009 Self-organization of a mesoscale bristle into ordered, hierarchical helical assemblies. *Science* **323**, 237–240.

PY, C., BASTIEN, R., BICO, J., ROMAN, B. & BOUDAOUD, A. 2007 3D aggregation of wet fibers. *Europhys. Lett.* **77**, 44005.

SHEPHERD, R. F., ILIEVSKI, F., CHOI, W., MORIN, S. A., STOKES, A. A., MAZZEO, A. D., CHEN, X., WANG, M. & WHITESIDES, G. M. 2011 Multigait soft robot. *Proc. Natl Acad. Sci. USA* **108** (51), 20400–20403.

SHEPHERD, R. F., STOKES, A. A., FREAKE, J., BARBER, J., SNYDER, P. W., MAZZEO, A. D., CADEMARTIRI, L., MORIN, S. A. & WHITESIDES, G. M. 2013 Using explosions to power a soft robot. *Angew. Chem.* **125** (10), 2964–2968.

STELTZ, E., MOZEIKA, A., RODENBERG, N., BROWN, E. & JAEGER, H. M. 2009 JSEL: jamming skin enabled locomotion. In *IEEE/RSJ International Conference Intelligent Robots and Systems, IROS 2009*, pp. 5672–5677. IEEE.

STOKES, A. A., SHEPHERD, R. F., MORIN, S. A., ILIEVSKI, F. & WHITESIDES, G. M. 2013 A hybrid combining hard and soft robots. *Soft Robot.* **1** (P), 70–74.

TOPPALADODDI, S. & BALMFORTH, N. J. 2014 Slender axisymmetric stokesian swimmers. *J. Fluid Mech.* **746**, 273–299.

ZHAO, Z., TAWFICK, S. H., PARK, S. J., DE VOLDER, M., HART, A. J. & LU, W. 2010 Bending of nanoscale filament assemblies by elastocapillary densification. *Phys. Rev.* E **82**, 041605.